EFFECTS OF PRETWIST AND PRESETTING ANGLES ON FREE VIBRATION OF ELASTICALLY TAILORED ROTATING THIN-WALLED BEAMS

S-Y Oh[†], L. Librescu[†] and O. Song[‡]
[†] Virginia Polytechnic Institute and State University
Department of Engineering Science and Mechanics
Blacksburg, Virginia 24061, USA
[‡] Chungnam National University
Mechanical Engineering Department
Taejon, 305-764, Korea

Keywords: *Free vibration; Thin-walled composte beams; Presetting and pretwist; Rotating beams; Shearable beam model.*

Abstract

A refined dynamic theory of rotating blades modeled as anisotropic composite thin-walled beams, experiencing the flapping-lagging-transverse shear coupling is presented. The structural model encompasses a number of non-standard features, such as anisotropy and transverse shear, pretwist and presetting angles, the presence of a rigid hub on which the beam is mounted, and the rotatory inertia. The developed theory and the methodology used to determine the eigenfrequency characteristics are validated against the results available in the literature, and new results emphasizing the influence played by the ply-angle, pretwist and presetting, coupled with that of the rotating speed on blade free vibration characteristics are supplied, and pertinent conclusions are outlined.

1 Introduction

The accurate prediction of free vibration characteristics of turbine blades, tilt rotor aircraft, helicopter blades and aircraft propellers is of a considerable importance towards the reliable design of these structural systems. A good knowledge of their free vibration characteristics is essential toward determination of their dynamic response to external excitations, resonant behavior, flutter instability and of their fatigue life.

In order to be able to predict adequately the free vibration response of advanced rotating blades constructed of composite materials, comprehensive structural models that encompass a number of features such as anisotropy and transverse shear, warping restraint, as well as the pretwist and presetting angles, should be developed and used. Traditionally, this problem, considered in specialized contexts, was approached within a *solid isotropic beam model*. In this sense, the reader is referred to the survey-paper by Rosen [1] where ample references to the literature addressing various related issues have been supplied. Within the concept of thin-walled beams, the treatment of the free vibration problem of rotating beams was carried out in various specialized contexts in a number of papers (see e.g. the most recent survey papers, by Jung et al. [2, 3], that provide extensive references on the state-of-the-art of this problem. In addition, extensive references can be found in the references [4] through [8].

However, in spite of the extensive work devoted to this problem, one should remark the

absence of a structural model of rotating thin-walled beams encompassing the basic features of advanced filamentary composite structural systems, such as directionality and transverse shear, as well as the pretwist and presetting effects. Within this paper, the coupled flapping-lagging-transverse shear vibrations of a pretwisted rotating composite thin-walled beam mounted on a rigid hub of radius R_0 at a setting angle γ, and featuring the previously mentioned effects are investigated.

In this context, the effects of the ply-angle of the filamentary constituent materials and of transverse shear, as well as that of the hub radius and angular velocity on coupled bending vibrations are addressed, and pertinent results are provided.

2 Analysis

2.1 Preliminaries

The case of a straight pretwisted flexible beam of length L mounted on a rigid hub of radius R_0, rotating at the constant angular velocity Ω as shown in Fig. 1 is considered. The beam is allowed to vibrate flexurally in a plane making an angle γ, referred to as setting angle with the plane of rotation. The origin of the rotating systems of coordinates (x,y,z) is located at the blade root, at an offset R_0 from the rotation axis. Besides the rotating coordinates (x,y,z), we also define the local coordinates $(x^p,\ y^p,\ z^p)$, where x^p and y^p are the *principal axes* of an arbitrary beam cross-section (see Refs. [6-8]). The two coordinate systems are related by the following transformation formulae:

$$\begin{aligned} x &= x^p \cos(\gamma+\beta(z)) - y^p \sin(\gamma+\beta(z)),\\ y &= x^p \sin(\gamma+\beta(z)) + y^p \cos(\gamma+\beta(z)),\\ z &= z^p \end{aligned} \tag{1a-c}$$

where $\beta(z) = \beta_0 z/L$ denotes the pretwist angle of a current beam cross-section, β_0 denoting the pretwist at the beam tip.

In addition to the previously defined coordinate systems, the inertial reference system (X,Y,Z) is attached to the center of the hub O. By $(\mathbf{i},\ \mathbf{j},\ \mathbf{k})$ and $(\mathbf{I},\ \mathbf{J},\ \mathbf{K})$ we define the unit vectors associated with the rotating and inertial coordinates, $(x,\ y,\ z)$ and (X,Y,Z), respectively. In addition, a local (surface) coordinate systems $(s,\ z,\ n)$ is considered. The geometric configuration and the typical cross-section, along with the associated systems of coordinates are presented in Figs. 1.

Within the present work, the precone angle of the blade is assumed to be zero. It is further assumed that the rotation takes place in the plane (X, Z) with the constant angular velocity $\Omega(\equiv \Omega\mathbf{J} = \Omega\mathbf{j})$, the spin axis being along the Y-axis.

The considered structural model corresponds to a single-cell thin-walled beam (TWB) of uniform closed-section, where the spanwise, z-coordinate axis coincides with a straight unspecified reference longitudinal axis.

2.2 Kinematics

The position vector of a point $M(x,y,z)$ belonging to the deformed beam structure is expressed as:

$$\mathbf{R}(x,y,z;t) = (x+u)\,\mathbf{i} + (y+v)\,\mathbf{j} + (z+w)\mathbf{k} + \mathbf{R}_0, \tag{2}$$

where x, y and z are the Cartesian coordinates of the points of the 3-D continuum in its undeformed state, while u, v and w denote displacement components. Recalling that the spin rate was assumed to be constant, keeping in mind that the rotation takes place solely in the XZ plane, and making use of equations expressing the time derivatives of unit vectors **(i, j, k)**, one obtain the velocity and acceleration vectors of an arbitrary point M of the beam under the form

$$\dot{\mathbf{R}} = V_x\mathbf{i} + V_y\mathbf{j} + v_z\mathbf{k} \tag{3a}$$

and

$$\ddot{\mathbf{R}} = a_x\mathbf{i} + a_y\mathbf{j} + a_x\mathbf{k} \tag{3b}$$

respectively. Their components are as follows:

$$\begin{aligned} V_x &= \dot{u} + (R_0 + z + w)\,\Omega;\ \ V_y = \dot{v};\\ V_z &= \dot{w} - (x+u)\Omega \end{aligned} \tag{4a-c}$$

and

$$a_x = \ddot{u} + \underline{2\dot{w}\Omega} - \underline{\underline{(x+u)\Omega^2}}; \quad a_y = \ddot{v},$$
$$a_z = \ddot{w} - \underline{2\dot{u}\Omega} - \underline{\underline{(R_0+z+w)\,\Omega^2}} \qquad (5a\text{-}c)$$

In these equations and the following ones, the superposed dots denote time derivatives, and the terms underscored by one or two superposed solid lines are associated with Coriolis and centrifugal inertia terms, respectively. As concerns the components of the displacement vector, their expressions have been supplied in Ref. [9], and are reproduced here for completion

$$\begin{aligned} u(x,t,z;t) &= u_0(z;t) - y\phi(z;t);\ v(x,y,z;t) \\ &= v_0(z;t) + x\phi(z;t), \\ w(x,t,z;t) &= w_0(z;t) + \theta_x(z;t)\left[y(s) - n\frac{dx}{ds}\right] \\ &\quad + \theta_y(z;t)\left[x(s) + n\frac{dy}{ds}\right] \qquad (6a\text{-}c) \\ &\quad - \phi'(z;t)[F_w(s) + na(s)]. \end{aligned}$$

In these equations $u_0(z;t), v_0(z;t), w_0(z;t)$ denote the rigid body translations along the x,y and z axes, while $\phi(z;t)$ and $\theta_x(z;t), \theta_y(z,t)$ denote the twist about the z-axis and rotations about the x and y-axes respectively. The expressions of θ_x and θ_y are

$$\theta_x(z;t) = \gamma_{yz}(z;t) - v_0'(z;t);$$
$$\theta_y(z;t) = \gamma_{xz}(z;t) - u_0'(z;t). \qquad (7a,b)$$

In Eqs. (6), $F_w(s)$ and $na(s)$ play the role of primary and secondary warping functions, respectively. For their definition, see e.g. Ref. [9].

In the absence of transverse shear effects where, γ_{xz} and γ_{yz} denote transverse shear strains,

$$\theta_x(z;t) = -v_0'(z;t);\ \theta_y(z;t) = -u_0'(z;t). \quad (8a,b)$$

In these equations, as well as in the forthcoming ones, the primes denote differentiation with respect to the longitudinal z-coordinate.

2.3 The Equations of Motion and Boundary Conditions

In order to derive the equations of motion and the associated boundary conditions, Hamilton's variational principle is used. This variational principle may be stated as (see Ref. [10]).

$$\delta J = \int_{t_0}^{t_1} \left[\int_\tau \sigma_{ij}\delta\varepsilon_{ij} d\tau - \delta K - \delta A - \int_\tau \rho H_i \delta v_i d\tau \right] dt = 0 \qquad (9)$$

where σ_{ij} and ε_{ij} stand for the 3-D stress and strain tensors, respectively,

$$U = \frac{1}{2}\int_\tau \sigma_{ij}\varepsilon_{ij} d\tau, \text{ and } K = \frac{1}{2}\int_\tau \rho(\dot{\mathbf{R}}\cdot\dot{\mathbf{R}}) d\tau \qquad (10a,b)$$

denote the strain energy functional and the kinetic energy, respectively.

In these equations, t_0 and t_1 denote two arbitrary instants of time; $d\tau(\equiv dndsdz)$ denotes the differential volume element, H_i denote the components of the body forces; ρ denotes the mass density; an undertilde sign identifies a prescribed quantity, while δ denotes the variation operator. In Eqs. (9) and (10) the Einstein summation convention applies to repeated indices, where Latin indices range from 1 to 3. In the same equations, $(v_1,v_2,v_3) \equiv (u,v,w)$, and $(x_1,x_2,x_3) \equiv (x,y,z)$.

As necessary pre-requisites, the various energies that are involved in the variational principle have to be rendered explicitly. Their expressions are not displayed in this paper. Hamilton's principle will also be used, to solve the resulting eigenvalue problems. This method is referred to as the Extended Galerkin Method [11].

3 Governing System

3.1 The shearable system

In the present paper a special case of ply-angle distribution inducing special elastic couplings will be considered. This consists of the lamination scheme

$$\theta(x) = \theta(-x), \quad \theta(y) = \theta(-y), \qquad (11)$$

where θ denotes the ply angle orientation considered to be positive when is measured from the positive s-axis towards the positive z-axis (see Fig. ()).

As it was previously shown, (see Atilgan and Rehfield [12]), this ply-angle configuration, referred to as the *Circumferentially Uniform Stiffness* configuration achievable via the usual filament winding technology, results in an exact decoupling between flapping- lagging-transverse shear, on one hand, and extension-torsional motion, on the other hand. In the present study only the former problem involving the bending-bending coupling will be considered.

The governing dynamical equations of pretwisted rotating blades expressed in terms of displacement variables are expressed as:

Herein, p_x, p_y, m_x and m_y are the external loads and moments that are assumed to be functions of both z and t coordinates.

$$\begin{aligned}
\delta u_0:\ & \big[a_{42}(z)\theta_y' + a_{43}(z)\theta_x' + a_{44}(z)(u_0' + \theta_y) \\
& + a_{45}(z)(v_0' + \theta_x)\big]' - b_1\ddot{u}_0 + \underline{\underline{b_1 u_0 \Omega^2}} \\
& + \underline{\underline{b_1\Omega^2[R(z)u_0']'}} + p_x = 0, \\
\delta v_0:\ & \big[a_{52}(z)\theta_y' + a_{53}(z)\theta_x' + a_{55}(z)(v_0' + \theta_x) \\
& + a_{54}(z)(u_0' + \theta_y)\big]' - b_1\ddot{v}_0 \\
& + \underline{\underline{b_1\Omega^2[R(z)v_0']'}} + p_y = 0, \qquad (12)\\
\delta\theta_y:\ & \big[a_{22}(z)\theta_y' + a_{25}(z)(v_0' + \theta_x) + a_{24}(z) \\
& (u_0' + \theta_y) + a_{23}(z)\theta_x'\big]' - a_{44}(z)(u_0' + \theta_y) \\
& - a_{43}(z)\theta_x' - a_{45}(z)(v_0' + \theta_x) - a_{42}(z)\theta_y' \\
& - \Big(b_5(z) + \delta_n b_{15}(z)\Big)\big(\underset{\cdots}{\ddot{\theta}_y} - \underline{\Omega^2\theta_y}\big) \\
& - \Big(b_6(z) - \delta_n b_{13}(z)\Big)\big(\underset{\cdots}{\ddot{\theta}_x} - \underline{\Omega^2\theta_x}\big) \\
& + m_y = 0, \\
\delta\theta_x:\ & \big[a_{33}(z)\theta_x' + a_{32}(z)\theta_y' + a_{34}(z)(u_0' + \theta_y) \\
& + a_{35}(z)(u_0' + \theta_x)\big]' - a_{55}(z)(v_0' + \theta_x) \\
& - a_{52}(z)\theta_y' - a_{54}(z)(u_0' + \theta_y) - a_{53}(z)\theta_x' \\
& - \Big(b_4(z) + \delta_n b_{14}(z)\Big)\big(\underset{\cdots}{\ddot{\theta}_x} - \underline{\Omega^2\theta_x}\big) \\
& - \Big(b_6(z) - \delta_n b_{13}(z)\Big)\big(\underset{\cdots}{\ddot{\theta}_y} - \underline{\Omega^2\theta_y}\big) \\
& + m_x = 0.
\end{aligned}$$

For the sake of identification, in the previous equations, the terms associated with the centrifugal acceleration terms are underscored by two superposed solid lines (====) ; rotatory inertia terms by a dotted line $(\cdots)$, and centrifugal-rotatory effect by a solid line superposed on a wavy line ($\approx$).

Assuming the blade to be clamped at z = 0 and free at z = L, the homogeneous boundary conditions result as:
At z = 0:

$$u_0 = 0,\ v_0 = 0,\ \theta_x = 0,\ \theta_y = 0, \qquad (13)$$

and at z = L:

$$\begin{aligned}
\delta u_0:\ & a_{42}(L)\theta_y' + a_{43}(L)\theta_x' + a_{44}(L)(u_0' + \theta_y) \\
& + a_{45}(L)(v_0' + \theta_x) = 0, \\
\delta v_0:\ & a_{52}(L)\theta_y' + a_{53}(L)\,\theta_x' + a_{55}(L)\,(v_0' + \theta_x) \\
& + a_{54}(L)(u_0' + \theta_y) = 0, \qquad (14)\\
\delta\theta_y:\ & a_{22}(L)\theta_y' + a_{25}(L)(v_0' + \theta_x) + a_{24}(L)(u_0' + \theta_y) \\
& + a_{23}(L)\theta_x' = 0, \\
\delta\theta_x:\ & a_{33}(L)\theta_x' + a_{34}(L)(u_0' + \theta_y) + a_{35}(L)(v_0' + \theta_x) \\
& + a_{32}(L)\theta_y' = 0.
\end{aligned}$$

As is clearly seen, these equations can address either the dynamic response of rotating blades exposed to time-dependent external excitation, or the free vibration problem. In the latter case, the external loads should be discarded.

In equations (12) and the following ones

$$R(z) \equiv [R_0(L - z) + \frac{1}{2}(L^2 - z^2)], \qquad (15)$$

whereas the coefficients $a_{ij}(z) = a_{ji}(z)$ and $b_i(z)$ denote stiffness and reduced mass terms, respectively. Their expressions are not displayed here.

3.2 Nonshearable Counterpart of the Previously Obtained System

Extracting from equations $(16)_3$ and $(16)_4$, the expressions $a_{44}(u_0' + \theta_y) + a_{45}(v_0' + \theta_x)$ and $a_{55}(v_0' + \theta_x) + a_{54}(u_0' + \theta_y)$, respectively, and their corresponding replacement in Eqs. $(16)_1$, $(16)_2$, $(18)_1$, and $(18)_2$ followed by consideration of $\theta_x \to -v_0'$ and $\theta_y = -u_0'$, yields

the Bernoulli-Euler counterpart of the shearable beam model. The corresponding equations will not be displayed here.

4 Comparisons with Available Numerical Predictions

The equations derived for the case of rotating *thin-walled beams* are similar to the ones corresponding to a *solid beam* model. The difference occurs only in the *proper* expression of cross-sectional stiffness quantities and mass terms. For this reason, use of dimensionless parameters in which these quantities are absorbed, enables one to obtain universal results, valid for both solid and thin-walled beams. In order to validate both the solution methodology and the structural model developed in this paper, comparisons with a number of results available in the literature are presented. The comparisions reveals an excellent agreement. These comparisons will not be supplied here.

5 Numerical Simulations and Discussion

Although the obtained equations are valid for a beam of arbitrary closed-cross section, for the sake of illustration the case of a rotating beam modelled as a composite box-beam (see Fig. 1) characterized by a cross-section ratio $R\,(\equiv c/b) = 5$ was considered.

In addition, unless otherwise specified, its dimensions are: L = 80in. (2.023m); c = 10in. (0.254m); b = 2in. (50.8 $\times 10^{-3}$m); h = 0.4in. (10.16 $\times 10^{-3}$m). The mechanical characteristics of the beam as considered in the numerical simulations correspond to the graphite/epoxy material. Its elastic characteristies can be found e.g. in Refs. [9]. As a result these are not supplied here.

$$
\begin{aligned}
E_L &= 30\times 10^6 psi(20.68\times 10^{10} N/m^2),\\
E_T &= 0.75\times 10^6 psi(5.17\times 10^9 N/m^2)\\
G_{LT} &= 0.37\times 10^6 psi(2.55\times 10^9 N/m^2),\\
G_{TT} &= 0.45\times 10^6 psi(3.10\times 10^9 N/m^2)\\
\mu_{TT} &= \mu_{LT} = 0.25;\\
\rho &= 14.3\times 10^{-5} lb.sec./in^4(1,528.15 kg/m^3)
\end{aligned}
$$

The eigenvalue problem was solved by using an exceptionally powerful methodology based on Extended Galerkin Method (see Ref. [11]).

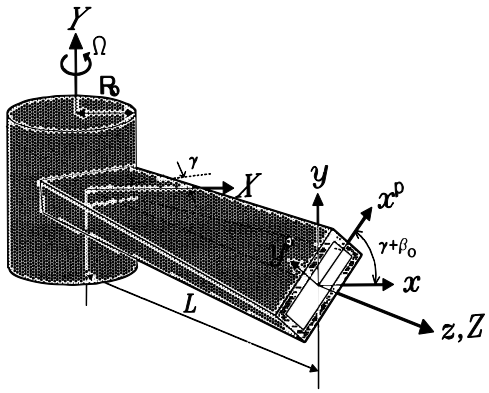

Fig. 1a Geometry of the pretwisted beam.

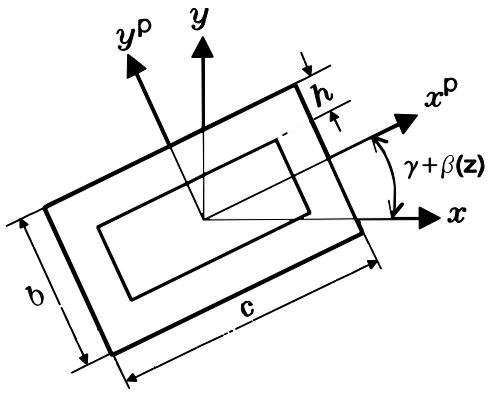

Fig. 1b Cross-section of the beam with pretwist and presetting angles.

Figures 2 and 3 display the variation of the first two natural frequencies of the rotating beam ($\Omega = 100\ rad/sec.$), as a function of the ply-angle, for selected values of the setting angle, and for the pretwist, β_0 = 90 deg.

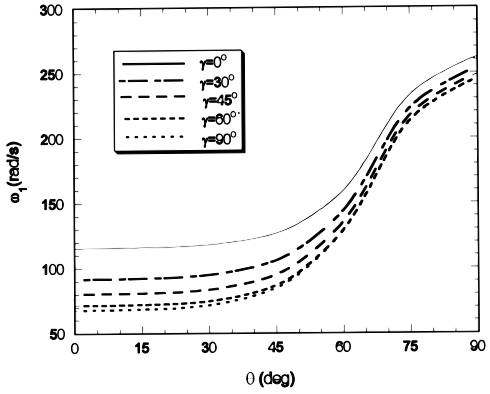

Fig. 2 Variation of the first coupled flapping-lagging natural frequency vs. ply angle for different setting angles (β_0 = 90 deg., Ω = 100 rad/sec., $\bar{R}_0$ = 0.1)

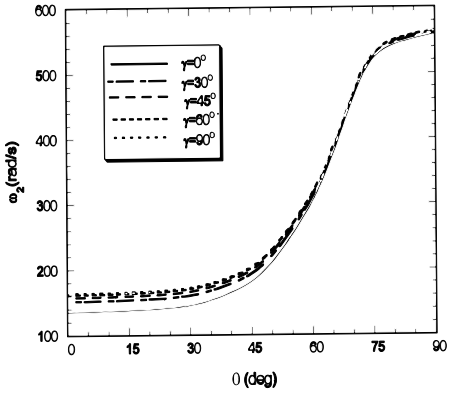

Fig. 3 Variation of the second coupled flapping-lagging natural frequency vs. ply angle for different setting angles. (β_0 = 90 deg., Ω = 100 rad/sec., $\bar{R}_0$ = 0.1)

The results reveal a continuous increase of natural frequencies that accompanies the increase of the ply-angle. Moreover, consistent with the results reported by the same authors but not displayed here, depending on the odd or even mode number, the increase of the presetting angle yields either a decrease or increase of natural frequencies.

Related to these results, one should remark from Figs. 4 and 5 that the increase of the rotational speed yields an increase of natural frequencies as compared to those displayed in Figs. 2 and 3, where a lower angular speed was considered. Moreover, at larger angular speeds, the effect of the ply-angle is more individualized for each of the considered setting angles than in the case of lower angular speeds.

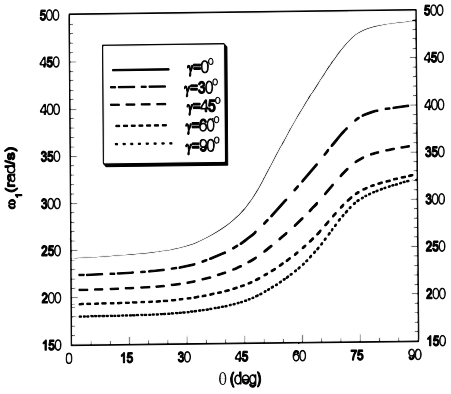

Fig. 4 The counterpart of Fig. 2 for Ω = 400 rad/sec.

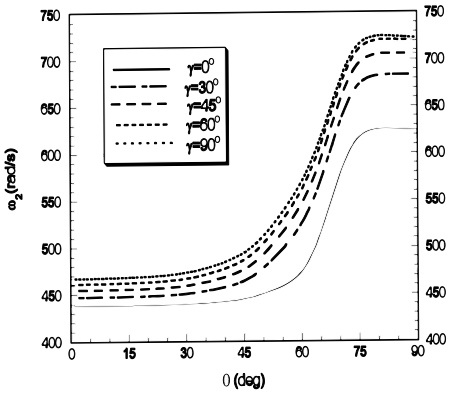

Fig. 5 The counterpart of Fig. 3 for Ω = 400 rad/sec.

In Figs. 6 through 8, there is displayed in succession the variation of the first three natural frequencies, as a function of the setting angle, for selected values of the rotational speed. As it clearly appears also from these figures, the effect of the setting angle on eigenfrequency of nonrotating beam is immaterial.

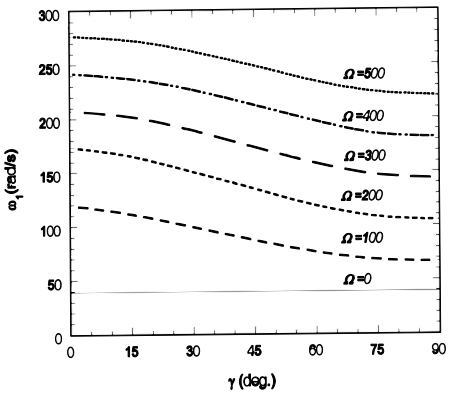

Fig 6 First coupled flapping-lagging natural frequency vs. presetting angle for selected rotational speeds (θ = 0, β_0 = 30 deg., $\bar{R}_0$ = 0.1)

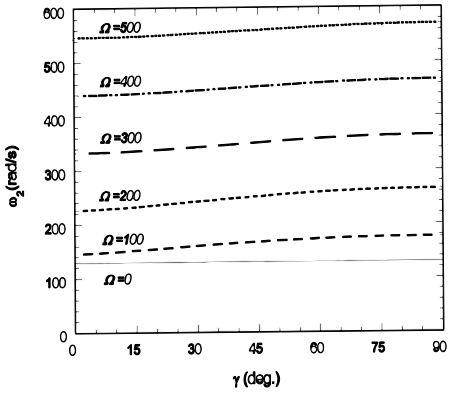

Fig. 7 Second coupled freqnecy vs. presetting angle for selected rotational speeds ($\theta = 0$, $\beta_0 = 30$ deg., $\bar{R}_0 = 0.1$)

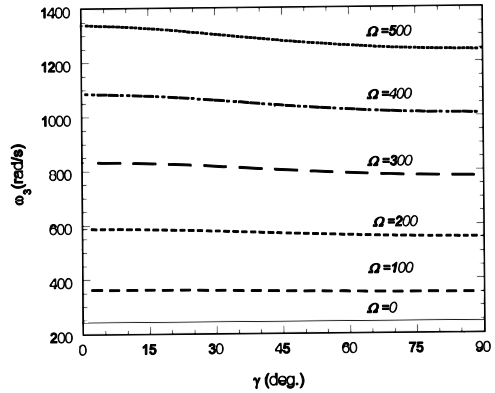

Fig. 8 Third coupled flapping-lagging natural frequency vs. presetting angle for selected rotational speeds ($\theta = 0$, $\beta_0 = 30$ deg., $\bar{R}_0 = 0.1$)

On the other hand, the trend of variaton of various mode frequencies as a function of the presetting angle and angular velocity remains similar to that previously emphasized. In these numerical simulations, the considered pretwist angle was $\beta_0 = 30$ deg. Results not displayed here obtained for the case of zero pretwist reveal that the pretwist has a relatively minor effect on the natural frequencies.

In Figs. 9 and 10, for selected values of the setting angle it is displayed in succession the variation of the first two natural frequencies, as a function of the pretwist angle. For zero presetting angle, the trend of variation of natural frequencies with that of the pretwist angle, coincides with that reported e.g. in the paper by Song et al. Refs. [6 and 8].

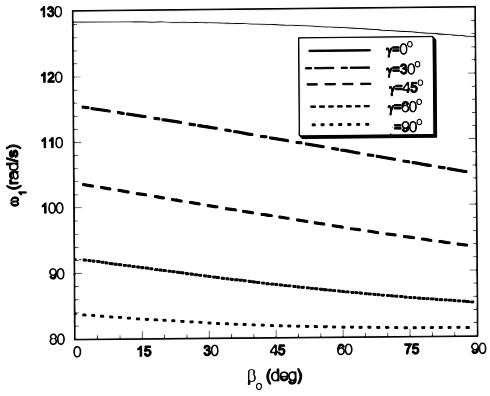

Fig. 9 Variation of the first coupled flapping-lagging natural frequency vs. pretwist angle for different setting angles of the rotating beam ($\theta = 45$ deg., $\Omega = 100$ rad/sec., $\bar{R}_0 = 0.1$)

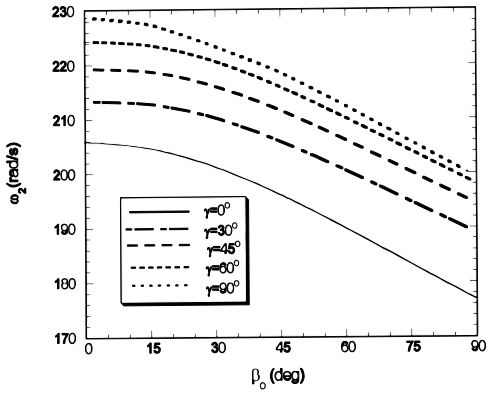

Fig. 10 Variaton of the second coupled natural frequency vs. pretwist angle for different setting angles of the rotating beam ($\theta = 45$ deg., $\Omega = 100$ rad/sec., $\bar{R}_0 = 0.1$)

In Figs. 11 and 12 there are displayed the implications of the hub radius, coupled with that of the rotating speed on the fundamental coupled flapping-lagging natural frequency, for the beam featuring, the setting angles $\gamma = 0$ and $\gamma = 90$ deg., and for the ply-angles, in succession, $\theta = 0$ and $\theta = 45$ deg., respectively. Due to the fact that in both cases, as considered in Figs. 11 and 12, the pretwist is $\beta_0 = 90$ deg., the flapping-lagging coupling is present also in the cases involving $\gamma = 0$ and $\theta = 0$.

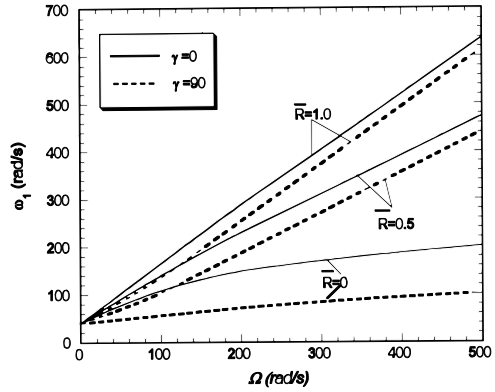

Fig. 11 Variation of the first coupled flapping-lagging natural frequency vs. the rotational speed for different hub radii and two setting angles (β_0 = 90 deg., θ = 0)

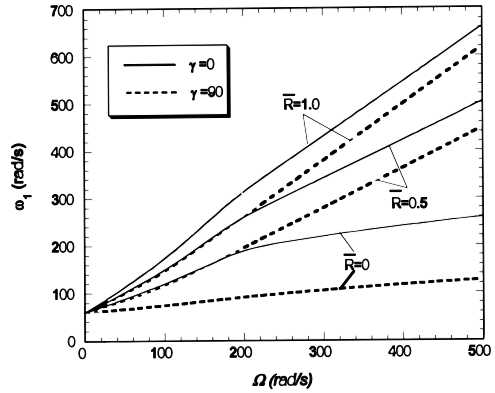

Fig. 12 The counterpart of Fig. 11 for the ply-angle θ = 45 deg.

The results reveal that the differences between the frequencies corresponding to $\gamma = 0$ and $\gamma = 90$ deg. tend to decay with the increase of the hub radius. At the same time, the results reveal that the increase of the ply-angle tends to exacerbate the difference between the frequencies corresponding to $\gamma = 0$ and $\gamma = 90$ deg., and associated to the same $\bar{R}_0$.

Figures 13 through 15 further emphasize the considerable role that the tailoring technique can play toward the increase, without weight penalties, of the coupled flapping-lagging natural frequencies of rotating beams. Such a role that renders the composite material systems overwhelmingly superior to the metallic structures, deserves well to be highlighted again in these graphs.

In addition, these plots reveal a number of trends related to the implications of the setting angle on each mode frequency, trends that have already been outlined in the previously displayed numerical simulations.

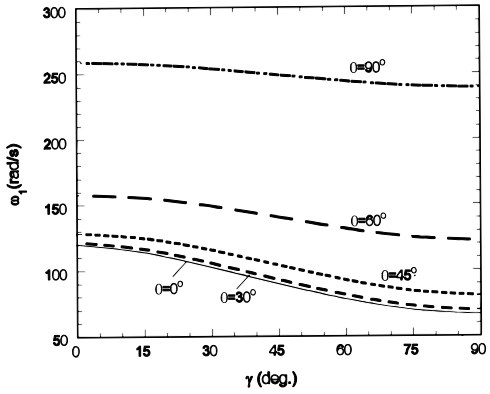

Fig. 13 First coupled flapping-lagging for selected ply-angles (β = 0, Ω = 100 rad/sec., $\bar{R}_0$ = 0.1)

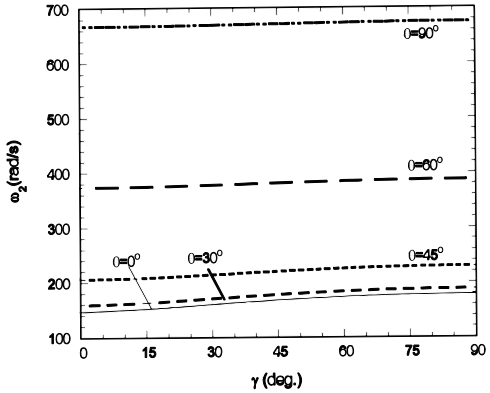

Fig. 14 Second coupled flapping-lagging natural frequency vs. presetting angle for selected ply-angles (β = 0, Ω = 100 rad/sec., $\bar{R}_0$ = 0.1)

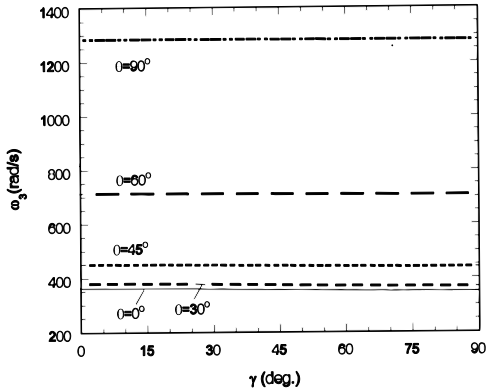

Fig. 15 Third coupled flapping-lagging natural frequency vs. presetting angle for selected ply-angles (β = 0, Ω = 100 rad/sec., $\bar{R}_0$ = 0.1)

6 Conclusions

A dynamic structural model of rotating thin-walled beams encompassing a number of non-classical effects was presented. The developed

structural beam model accounts for the effects of the directionality of the fibrous composite materials, and of the elastic couplings induced thereof, transverse shear, rotatory inertias, and of the hub radius. In addition, the effects played by the pretwist and presetting angles, coupled with the previously mentioned ones have been incorporated and their implications on free vibration have been revealed.

Comparisons of eigenfrequency predictions based on the developed model and the Extended Galerkin Solution Methodology used in this paper with some available theoretical and experimental ones for rotating and non- rotating beams have been carried out, and excellent agreements have been reached.

It is hoped that the results reported here will be helpful toward a better understanding of the implications of a number of non-classical effects on natural frequencies of advanced rotating beams, and toward the validation of the finite element and of other approximate methods that are used in the context of the dynamics of rotating beams.

References

[1] Rosen, A., "Structural and dynamic behavior of pretwisted rods and beams," *Applied Mechanics Reviews*, **44**, 12, Part 1, pp. 483-515, 1991.

[2] Jung, S. N., Nagaraj, V. T., and Chopra, I., "Assessment of composite rotor blade: modeling techniques," *Journal of the American Helicopter Society*, Vol. 44, No. 3, pp. 188-205, 1999.

[3] Jung, S. N., Nagaraj, V. T. and Chopra, I., "Refined structural dynamics model for composite rotor blades," *AIAA Journal*, Vol. 39, No. 2, pp. 339-348, 2001.

[4] Song, O. and Librescu, L., "Structural modeling and free vibration analysis of rotating composite thin-walled beams," *Journal of the American Helicopter Society,* Vol. 42, No. 4, pp. 358-369, 1997.

[5] Song, O. and Librescu, L., "Modeling and dynamic behavior of rotating blades carrying a tip mass and incorporating adaptive capabilities," *Acta Mechanica,* Vol. 134, pp. 169-197, 1999.

[6] Song, O., Librescu, L. and Oh, S-Y., "Vibration of pretwisted adaptive rotating blades modeled as anisotropic thin-walled beams," *AIAA Journal*, Vol. 39, No. 2, February, pp. 285-295, 2001.

[7] Song, O., Librescu, L., and Oh, S.-Y, "Dynamic of pretwisted rotating thin-walled beams operating in a temperature environment," *Journal of Thermal Stresses*, Vol. 24, No. 3, pp. 255-279, 2001.

[8] Song, O., Oh, S-Y, and Librescu, L., "Dynamic behavior of elastically tailored rotating blades modeled as pretwisted thin-walled beams and incorporating adaptive capabilities," *International Journal of Rotating Machinery,* Vol. 8, No. 1, pp. 13-25, 2002.

[9] Song, O. and Librescu, L., "Free vibration of anisotropic composite thin-walled beams of closed cross-section contour," *Journal of Sound and Vibration*, **167**, (1), pp. 129-147, 1993.

[10] Librescu, L., "Elastostatics and kinetics of anisotropic and heterogeneous shell-type structures, Noordhoff International Publishing, Leyden, Netherlands, pp. 560-598, 1975.

[11] Librescu, L., Meirovitch, L. and Na, S. S., "Control of cantilevers vibration via structural tailoring and adaptive materials," *AIAA Journal*, Vol. 35, No, 8, August, pp. 1309-1315, 1997.

[12] Rehfield, L. W., Atilgan, A. R. and Hodges, D. H., "Nonclassical behavior of thin-walled composite beams with closed cross sections," *Journal of the American Helicopter Society,* Vol. 35, No. 2, pp. 42-51, 1990.